

X-RAY LUMINOSITY FUNCTIONS OF ACTIVE GALACTIC NUCLEI

TAKAMITSU MIYAJI

*Physics Department, Carnegie Mellon University
5000 Forbes Ave., Pittsburgh, PA 15213, USA
E-mail: miyaji@cmu.edu*

In this proceedings paper, I overview the current status of the X-ray luminosity function of AGNs in the soft (0.5-2 keV) band, extended using *XMM-Newton* and *Chandra* survey data. We found that the number density of low luminosity AGNs peaks later in the history of the universe ($z \sim 1$) than the that of high luminosity AGNs ($z \sim 1.7 - 3$). I also describe the basic results of a spectroscopic followup project of a complete *HEAO-1* hard X-ray limited sample of AGNs using *ASCA* and *XMM-Newton* and present separate intrinsic hard X-ray luminosity functions for unabsorbed and absorbed AGNs. We found that the absorbed AGN XLF drops more rapidly at high luminosities, indicating a deficiency of absorbed luminous AGNs.

1. Introduction

X-ray surveys are practically the most efficient means of finding active galactic nuclei (AGNs) over a wide range of luminosity and redshift. In order to construct an X-ray luminosity function (XLF) of AGNs, enormous efforts have been made to follow up X-ray sources with optical telescopes to establish their nature as AGNs and to measure their redshifts. Now that we have fairly complete samples of X-ray selected AGNs over 6 orders of magnitude in flux, from surveys ranging from all the high galactic latitude sky to the deepest pencil-beam fields. These enable us to construct and probe luminosity functions over cosmological timescales.

In this proceedings article, I overview the current progress of a few projects related to AGN XLF. Firstly, I overview the results of the soft X-ray (0.5-2 keV) luminosity function (SXLF), which is the continuation of our previous work with *ROSAT* samples¹¹, extended with deep *XMM-Newton* and *Chandra* surveys.

While the soft X-ray surveys select against obscured AGNs, in the current situation, the number of available objects and area-flux coverage from

extensive surveys make them useful for probing detailed behaviors of XLFs of the unabsorbed portion of the AGN activity. A complementary XLF in the hard band (2-10 keV) (HXLF) enables us to also look into obscured AGNs, and thus it provides most direct measure of the accretion onto supermassive blackholes (SMBHs). Ueda et al. in this volume covers our extensive recent work on HXLF (see also Ueda et al. 2003²⁰ for a full description).

In this article, we also present the results of our *XMM-Newton* and *ASCA* spectroscopic followup of a complete hard X-ray flux-limited sample of bright AGNs selected from *HEAO-1* catalogs¹⁹, the basic results of which have been integrated in the Ueda et al's HXLF.

2. AGN Soft X-ray Luminosity Function and Evolution

2.1. *The Combined Sample*

In addition to the *ROSAT* samples used in our previous work^{11,12}, we have added AGNs from the *ROSAT* North Ecliptic Pole Survey (NEPS)⁶, from an *XMM-Newton* observation on the Lockman Hole⁸ and the *Chandra* Deep Surveys South¹⁷/North². For the Lockman Hole region, the inner part based on the *ROSAT* HRI has been replaced by a new *XMM-Newton* sample⁸. Four medium-deep *ROSAT* surveys used in our previous work^{11,12}, i.e., the UK Deep Survey⁹, Marano Field²², North Ecliptic Pole (deep PSPC-pointing)³ and the outer part of the Lockman Hole (PSPC)¹⁵ are now collectively called the *ROSAT* Medium-Sensitivity Survey (RMS). The combined area versus limiting flux relation and the redshift-luminosity diagram are shown in Fig. 1. The samples are summarized in Table 1. We have tried to limit our analysis to “type 1” AGNs (including narrow-line Seyfert 1 galaxies). In the *ROSAT* samples, we selected type 1 AGNs mainly from the optical classifications. For the *XMM-Newton* Lockman Hole and *Chandra* DEEP field samples, the optical classification is supplemented by hardness ratios of the X-ray sources. AGNs with $z < 0.015$ have been excluded from the analysis to avoid the possible effects of the local large scale structure. Details will be explained in Hasinger et al. (in preparation).

2.2. *SXLF and Evolution with Redshift*

The soft X-ray Luminosity functions (SXLF) in different redshift bins have been calculated using the $N^{\text{obs}}/N^{\text{mdl}}$ estimator, where each redshift bin

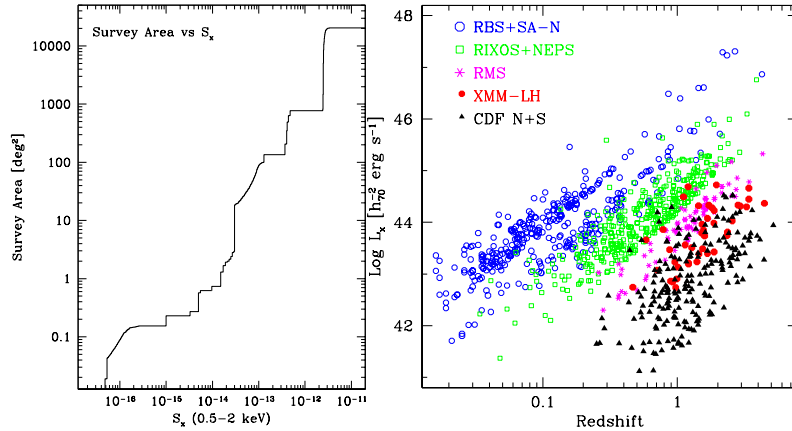


Figure 1. *Left*: The survey area of the combined soft X-ray sample as a function of flux. *Right*: The soft X-ray sample in the z - $\text{Log } L_x$ plane.

Table 1. The Soft X-ray Sample

Survey	Area [deg ²]	$S_{x14,lim}$ [cgs]	N_{AGN}	Survey	Area [deg ²]	$S_{x14,lim}$ [cgs]	N_{AGN}
RBS ¹⁶	$2 \cdot 10^4$	≈ 250	203	RMS ^{9,22,15}	1.-0.5	.74-.32	83
SA-N ¹	684.-35.	47.-13.	134	LH-XMM ⁸	.33-.10	.13-.08	42
NEPS ⁶	80.-0.35	80.-1.5	162	CDF-S ¹⁷	.09-.02	.06-.02	115
RIXOS ¹⁰	19.-16.	8.5-3.0	196	CDF-N ²	.09-.02	.06-.005	97

has been maximum-likelihood fitted with a smoothed two power-law form and the model value at the center of each bin is multiplied by the ratio of the actual number of AGNs in the bin to the model-predicted number¹². Nominally, corrections for incompleteness due to unidentified X-ray sources have been made by using an *effective* survey area, derived by multiplying the geometrical survey area by the completeness of the survey (i.e. identified fraction of the detected X-ray sources). This method is valid when sources remain unidentified because of random reasons that are not correlated with the intrinsic properties of the source (e.g. optical magnitude). This is not necessarily true, especially in the deepest surveys. Thus we also calculated the XLF or number density upper bounds, where all the unidentified *XMM-Newton* and *Chandra* sources are assigned (in duplicate) the central redshift of each bin. Figure 2 (left) shows the SXLf in different redshift bins (plotted only the nominal incompleteness correction case).

Figure 2 (right) shows the AGN number densities as a function of red-

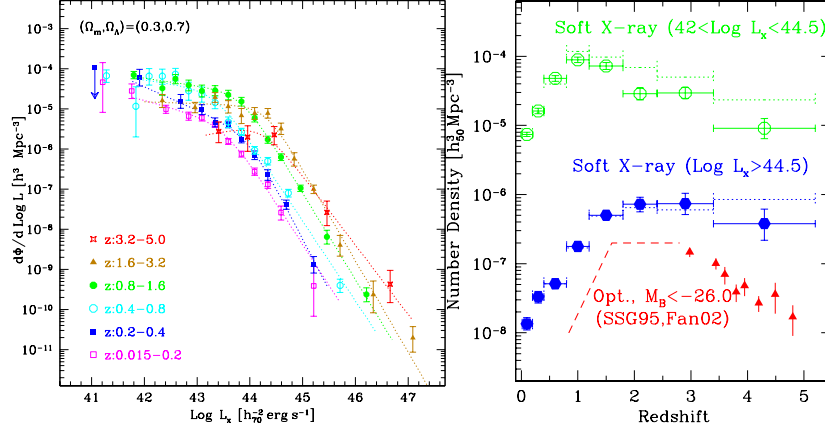


Figure 2. *Left:* The SXLf for different redshift bins, calculated using the $N^{\text{obs}}/N^{\text{mdl}}$ method. Errors bars corresponds to Poisson 1σ errors. *Right:* The number densities of soft X-ray selected AGNs with luminosities below and above $\text{Log } L_x = 44.5 \text{ erg s}^{-1}$. The same curve for optically-selected QSOs with $M_B < -26.0$ are shown. The $(\Omega_m, \Omega_\Lambda) = (1, 0)$ cosmology is used in this plot for historical comparisons.

shift separately for low and high luminosity AGNs. The incompleteness upper bounds (see above) are shown in dotted lines. Even in the most extreme cases of the incompleteness correction, we see that the number density of the low-luminosity AGNs peaks much later in the history of the universe ($z \sim 1$) than the high-luminosity case. This is in the opposite sense to the prediction from an analytical model based on the hierarchical merging and self-regulated accretion by Wyithe & Loeb²¹. According to their prediction, the number density of more luminous AGNs peak at later in the history of the universe. On the other hand, a prediction from a numerical simulation by Di Matteo et al.⁴, where gas density, star formation, and AGN formations are assumed to be related in a certain simple way, is consistent with the observed trend.

For comparison, we overplot the redshift evolution of optically-selected luminous ($M_B < -26$) QSO number density^{14,5}. In the high X-ray luminosity bin, we are not still certain (within the uncertainties in the incompleteness correction) whether we have detected the decline (with z) in the number density at $z > 2.7$, where the densities of luminous optical^{14,5} and radio¹⁸ QSOs clearly show a drop. Note, however, that when we take a different method on incompleteness correction involving optical magnitude limits with our soft X-ray sample, a density decline at $z > 2.7$ is preferred even for the high-luminosity sample (Hasinger et al. in preparation).

3. The Brightest Hard X-ray Sample

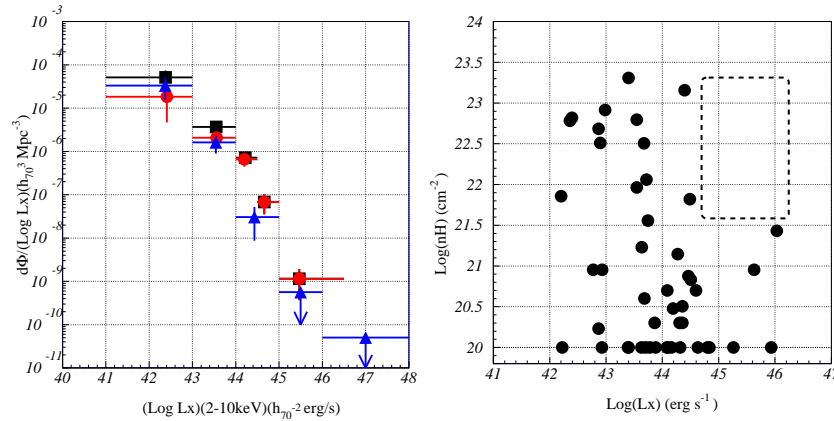


Figure 3. *Left:* The local *de-absorbed* HXLF (2-10 keV) of unabsorbed ($\text{Log } N_{\text{H}} \text{ cm}^{-2} \leq 21.5$; filled circle) and absorbed (> 21.5 ; filled triangle) AGNs. The open squares show the sum of both. *Right:* Intrinsic absorption of the sample AGNs are plotted against the intrinsic (de-absorbed) luminosity. There would be ~ 9 objects in the region enclosed by a thick dashed line if absorbed and unabsorbed AGNs intrinsic HXLFs were the same besides normalizations.

In order to construct the luminosity function of AGNs in the *intrinsic* X-ray luminosity, X-ray surveys in the hard band ($E > 2$ keV) and X-ray spectroscopic (or at least hardness) information are crucial. In order to complement deeper *ASCA*, *XMM-Newton* and *Chandra* surveys with smaller survey areas, we have defined a bright hard X-ray selected sample from the *HEAO-1* all-sky surveys. In addition to the famous Piccinotti et al.¹³ sample from the *HEAO-1* A2 experiment, we have defined a somewhat deeper hard X-ray flux-limited sample of AGNs from the MC-LASS catalog of X-ray sources from the *HEAO-1* A1/A3 experiments^a in a limited region. The AGN sample from the latter catalog was investigated in detail by Grossan⁷. As a total, 49 AGNs are defined and we have made spectral analysis of all of them (except one) using *ASCA* and *XMM-Newton* observation from archive as well as our own proposals. We have determined the intrinsic absorption N_{H} and underlying power-law index Γ . This enabled us to construct separate local HXLFs for absorbed and unabsorbed AGNs as functions of de-absorbed (intrinsic) luminosity (Fig. 3, left). We see that

^ahttp://heasarc.gsfc.nasa.gov/docs/heao1/archive/heao1_catalog.html

the absorbed AGN HXLF drops more rapidly than the unabsorbed one at high luminosities. This can also be demonstrated in the $L_x - N_H$ plot (Fig. 3, right). Suppose absorbed and unabsorbed AGNs had the same HXLF shape, there would be ~ 9 AGNs in the region enclosed by a thick dashed line in this figure. See Shinozaki et al.¹⁹. Full results will be reported by Shinozaki et al. (in preparation).

Acknowledgments

I thank my collaborators on the projects described in this article, especially Günther Hasinger, Maarten Schmidt, Keisuke Shinozaki, Yoshitaka Ishisaki and Yoshihiro Ueda. I thank the conference organizers for the invitation to give a talk. This work has been supported by the NASA LTSA grant NAG5-10875.

References

1. I. Appenzeller et al. *A&A*, **364**, 443 (2000)
2. A. Barger et al. *AJ*, **126**, 632 (2003)
3. R.G. Bower et al. *MNRAS*, **281**, 59 (1996)
4. T. Di Matteo et al. *ApJ*, **593**, 56 (2003)
5. X. Fan et al. *AJ*, **121**, 54 (2001)
6. I.M. Gioia et al. *ApJS*, **149**, 29 (2003)
7. B. Grossan PhD Thesis, MIT (1992)
8. V. Mainieri et al. *A&A*, **393**, 425 (2002)
9. I.M. McHardy et al. *MNRAS*, **295**, 641 (1998)
10. K.O. Mason et al. *MNRAS*, **311**, 456 (2000)
11. T. Miyaji, G. Hasinger, M. Schmidt *A&A*, **353**, 25 (2000)
12. T. Miyaji, G. Hasinger, M. Schmidt *A&A*, **369**, 49 (2001)
13. G. Piccinotti et al. *ApJ*, **253**, 485 (1982)
14. M. Schmidt, D.P. Schneider, J. Gunn *AJ*, **110**, 68 (1995)
15. M. Schmidt et al. *A&A*, **329**, 495 (1998)
16. A. Schwobe et al. *AN*, **321**, 1 (2000)
17. G.P. Szokoly et al. *ApJS* submitted (astro-ph/0312324) (2004)
18. P.A. Shaver et al. *Nature*, **384**, 439 (1996)
19. K. Shinozaki, T. Miyaji, Y. Ishisaki, Y. Ueda et al. in Proceedings of the "Stellar-Mass, Intermediate-Mass, and Supermassive Black Holes" in press (2004) (astro-ph/0402363)
20. Y. Ueda, M. Akiyama, K. Ohta, T. Miyaji *ApJ*, **598**, 886 (2003)
21. J.S.B. Wyithe, A. Loeb *ApJ*, **595**, 614 (2003)
22. G. Zamorani et al. *A&A*, **346**, 731 (1999)